Long-Distance Single Photon Transmission from a Trapped Ion via Quantum Frequency Conversion

Thomas Walker,[1] Koichiro Miyanishi,[2] Rikizo Ikuta,[2] Hiroki Takahashi,[1] Samir Vartabi Kashanian,[1] Yoshiaki Tsujimoto,[3] Kazuhiro Hayasaka,[3] Takashi Yamamoto,[2] Nobuyuki Imoto,[2] and Matthias Keller[1]

[1]*Department of Physics and Astronomy, University of Sussex, Brighton BN1 9RH, United Kingdom*

[2]*Graduate School of Engineering Science, Osaka University, Toyonaka, Osaka 560-8531, Japan*

[3]*Advanced ICT Research Institute, National Institute of Information and Communications Technology (NICT), Koganei, Tokyo 184-8795, Japan*

(Received 20 December 2017; published 15 May 2018)

Trapped atomic ions are ideal single photon emitters with long-lived internal states which can be entangled with emitted photons. Coupling the ion to an optical cavity enables the efficient emission of single photons into a single spatial mode and grants control over their temporal shape. These features are key for quantum information processing and quantum communication. However, the photons emitted by these systems are unsuitable for long-distance transmission due to their wavelengths. Here we report the transmission of single photons from a single $^{40}Ca^{+}$ ion coupled to an optical cavity over a 10 km optical fiber via frequency conversion from 866 nm to the telecom *C* band at 1530 nm. We observe nonclassical photon statistics of the direct cavity emission, the converted photons, and the 10 km transmitted photons, as well as the preservation of the photons' temporal shape throughout. This telecommunication-ready system can be a key component for long-distance quantum communication as well as future cloud quantum computation.

DOI: 10.1103/PhysRevLett.120.203601

The accessibility of matter quantum systems to standard telecommunication wavelengths is a prerequisite for long-distance optical fiber quantum networks, where matter systems play an important role in storing and providing nonclassical states of light [1]. Trapped ions coupled to optical cavities as individual qubit systems have been used to demonstrate single photon emission with controlled temporal shapes [2] and polarization [3] and the entanglement of ions and photons [4] prerequisites for quantum information processing [5,6] and quantum communication [7,8]. Until recently, however, the emission wavelength was limited by the internal structure of the ions. Often in the visible or near-infrared (NIR) regions, use of this emission is impractical over long distances due to the high attenuation in optical fibers. Furthermore, communication between disparate quantum systems was impossible due to their mismatched emission and absorption wavelengths. Quantum frequency conversion (QFC), which shifts the frequency of a photon without disturbing its quantum properties, is a solution to these issues. Since the first proposal of QFC [9], conversions between a wide range of frequencies have been demonstrated. Initially, this was used for detecting telecom photons with silicon photon detectors, which are usually confined to the visible and NIR regions [10]. Quantum state preservation has been demonstrated in a conversion between the NIR and telecom bands [11–13]. Furthermore, it has been applied to semiconductor quantum dots [14,15] and atomic ensembles [16–19]. Recently, a QFC system was employed to generate entanglement between a trapped ion and a frequency-converted photon [20]. In contrast to systems based on spontaneous emission, the emission of trapped ions coupled to an optical cavity can be coherently controlled and provides highly efficient emission into a single spatial mode. The ability to control the temporal shape of emitted photons is vital for a quantum interface to transfer entanglement between different systems. In this Letter, we demonstrate QFC of photons from a single ion coupled to an optical cavity from 866 to 1530 nm and the transmission of the converted photons through a 10 km optical fiber.

The ion trap is similar to that described in Ref. [21] and is shown in Fig. 1. $^{40}Ca^{+}$ ions are trapped in a linear Paul trap, in which symmetric radio frequency (rf) voltages on four blade-shaped electrodes form the radial trapping potential with a secular frequency of 1.23 MHz and dc voltages on two end cap electrodes provide axial confinement with a secular frequency of 760 kHz. The distance between the tips of the rf electrodes and trap center is 475 μm, and the dc electrodes are separated by 5 mm. The ion is coupled to an optical cavity formed by two mirrors, which are placed inside the end cap electrodes such that the cavity axis is collinear with the trap axis. One mirror with a transmissivity of 100 ppm at 866 nm acts as an output coupler, with the second mirror at 5 ppm leading to a finesse of 60 000. The cavity length is 5.3 mm, leading to an ion-cavity coupling strength of $g_0 = 2\pi \times 0.9$ MHz. A weak magnetic field of 0.5 G directed along the cavity axis defines the quantization axis for the ion without causing significant Zeeman splitting.

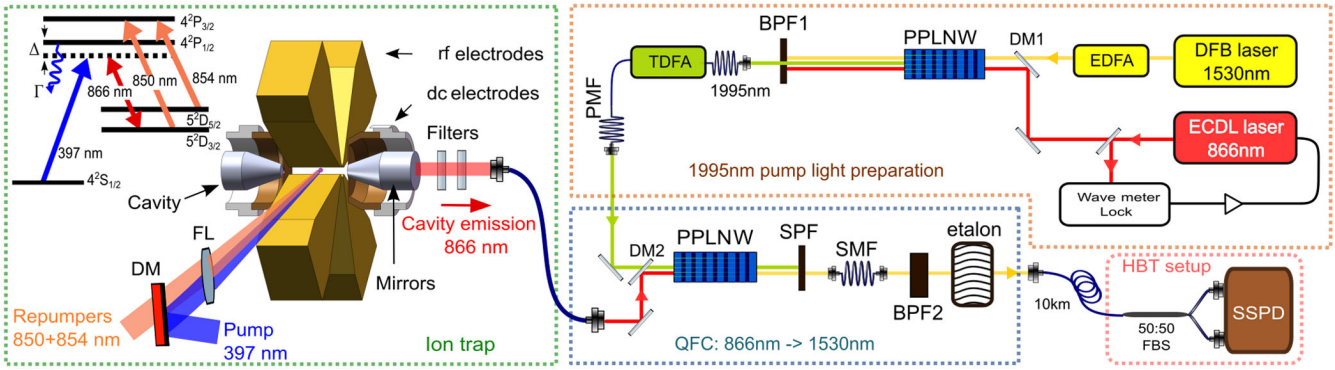

FIG. 1. The ion trap setup and $^{40}Ca^{+}$ level scheme is shown on the left. Lasers overlapped at a dichroic mirror (DM) and focused to the trap center by a lens (FL). The cavity length is stabilized via a reference laser locked to the D_1 transition of Cs at 894 nm. After a pair of longpass filters attenuate the 894 nm locking light to within the background rate of the detectors, the 866 nm cavity emission is coupled into a single-mode optical fiber, after which it may be coupled to a HBT setup for 866 nm photons or to the QFC setup as shown. The optical circuit for QFC is composed of two blocks: 1995 nm pump light preparation and QFC from 866 to 1530 nm. This is, in turn, connected to a HBT setup either directly or via a 10 km optical fiber.

The single photons were generated in a 10 μs sequence as shown in Fig. 2. The level scheme for $^{40}Ca^{+}$ is shown in Fig. 1. First, the ion is Doppler cooled using a laser red-detuned by $\Gamma/2$ ($\Gamma = 2\pi \times 22$ MHz) from resonance with the $^2S_{1/2} - {}^2P_{1/2}$ transition at 397 nm. Lasers at 850 and 854 nm are used to repump the ion out of the metastable $^2D_{3/2}$ state back into the cooling cycle. After cooling for 5.5 μs, the cooling beam is switched off for 1 μs to prepare the ion in the $S_{1/2}$ state. Then, a pulse of 397 nm light with a Gaussian temporal intensity profile drives a cavity-assisted Raman transition between the $^2S_{1/2}$ and $^2D_{3/2}$ states, producing an 866 nm photon in the cavity (similar to Ref. [2]). The photon emitted from the cavity is circularly polarized with a roughly equal probability of left or right handedness. The 1 s lifetime of the $^2D_{3/2}$ state ensures that only a single photon may be produced. A brief delay before and after the single photon drive pulse ensures the complete switch off of all laser repopulation of the $^2S_{1/2}$ and the generation of multiple photons. Using this scheme, the probability of generating and detecting a single photon is $(1.63 \pm 0.04)\%$ using the superconducting single photon detectors (SSPDs) as described later.

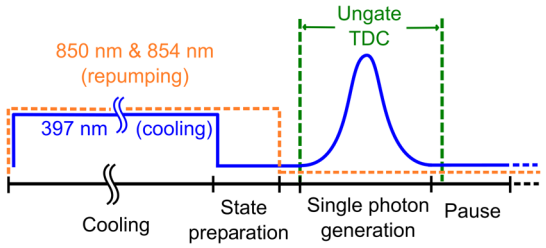

FIG. 2. This figure shows the sequence and shapes of laser pulses used to generate single photons (not to scale). The ion is initially cooled for 5.5 μs and then pumped into the $S_{1/2}$ state for 1 μs. After a brief delay, a Gaussian-shaped pulse drives a cavity-assisted Raman transition to produce a single photon, during which time the time-to-digital converter (TDC) records photon arrive times. The sequence is repeated at 99.6 kHz.

To convert the single photons from the ion to the telecom C band, a QFC setup was built and connected between the trap and a Hanbury Brown–Twiss (HBT) setup for 1530 nm light. The QFC system uses difference frequency generation (DFG) between the photons at 866 nm and strong 1995 nm pump light to generate 1530 nm photons. The full quantum frequency conversion setup is shown in Fig. 1, which is composed of two optical circuits: one for 1995 nm pump light preparation and one for QFC of the 866 nm photons to 1530 nm. At the pump light preparation stage, the 1530 nm light from a distributed feedback (DFB) laser with a linewidth of 10 MHz is amplified by an erbium-doped fiber amplifier (EDFA) to a maximal power of 450 mW. The light at 866 nm from an external cavity diode laser (ECDL) is locked at a frequency resonant with the transition of $^2D_{3/2} - {}^2P_{1/2}$ of Ca^{+} using a wave meter. The 866 nm and 1530 nm lasers are combined at a dichroic mirror (DM1) and coupled into a periodically poled lithium niobate waveguide (PPLNW). The 1995 nm light is prepared via DFG of 866 nm light with a strong pump light at 1530 nm. Using a bandpass filter (BPF1) with a center wavelength at 2000 nm and a bandwidth of 50 nm, the 1530 nm pump light and the remaining seed light at 866 nm are filtered out from the output. The extracted 1995 nm light is coupled to a polarization-maintaining fiber (PMF) and is amplified by a thulium-doped fiber amplifier (TDFA) to a maximum power of 1 W.

At the QFC stage, the amplified vertically (V) polarized 1995 nm pump light is injected to another PPLNW. The 866 nm photons from the ion-cavity system are combined with the pump by a dichroic mirror (DM2) and coupled to the PPLNW. After the PPLNW, the strong pump is eliminated by a short pass filter (SPF), and the converted

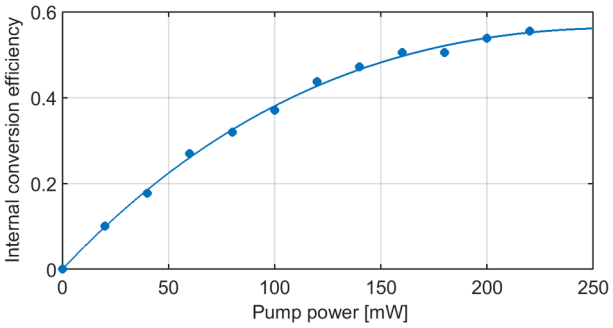

FIG. 3. The internal conversion efficiency from 866 to 1530 nm. A solid curve is obtained by the best fit to the experimental data with a function $A\sin^2(\sqrt{BP})$, where P is the power of the pump light at 1995 nm and the fitting parameters A and B are 0.56 and 9.3/W, respectively.

1530 nm photons are coupled into a single-mode fiber (SMF). The SMF is connected to a frequency filter circuit, consisting of a fiber-coupled bandpass filter (BPF2) with a bandwidth of 0.2 nm and an etalon with a FWHM of ~700 MHz for suppressing noise photons picked up through the QFC system. After the filters, the light is coupled to a SMF.

The conversion efficiency of the QFC system was characterized using V-polarized laser light at 866 nm from the ECDL. The coupling efficiency of the 866 nm light to the PPLNW is 80%. The conversion efficiency from 866 nm light to 1530 nm depends on the pump power used, as shown in Fig. 3. The maximum conversion efficiency is about 50% at 0.2 W effective pump power. The coupling efficiency of the converted light to the SMF is 60%. The peak transmittance of the frequency filters (BPF2 and the etalon) is 14% including fiber coupling. A pump power of 170 mW was used for the experiment, for which the internal conversion efficiency is ~50%. As a result, the total efficiency is about 3%.

To confirm that the system is a single photon source, the second-order intensity correlation function $g^{(2)}$ is measured using a HBT setup. The classical limit is $g^{(2)}(0) > 1$, whereas a single photon source has $g^{(2)}(0) = 0$. A fiber-based 50/50 beam splitter (FBS) directs the cavity emission onto two SSPDs with a specified quantum efficiency of > 80% at 850 nm (single-element nanowire detector from Photonspot Inc.). Similarly, after the QFC circuit, the 1530 nm photons are measured with a HBT setup using SSPDs with a specified quantum efficiency of > 80% at 1550 nm.

The electronic output pulses of the detectors are then recorded on two channels of a time-to-digital converter (TDC) (MCS6A from FastComtec). The difference in arrival times of photons in each channel are sorted into 200 ns bins, resulting in a histogram as shown in the inset in Fig. 4(a). The series of regular sharp peaks with a suppressed peak at zero delay is characteristic of a pulsed

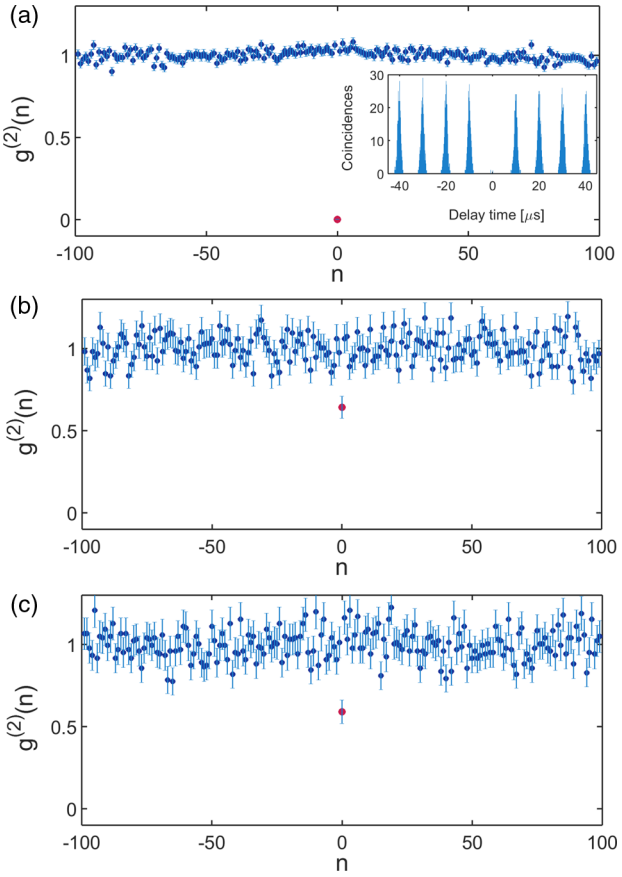

FIG. 4. The $g^{(2)}$ for delays up to 1 ms for (a) the 866 nm photons, (b) 1530 nm photons, and (c) 1530 nm photons with the 10 km fiber. The value at zero delay (shown in red) is clearly separated from the values at $n \neq 0$ in all cases, demonstrating sub-Poissonian statistics. The inset in (a) is for the coincidence events at 866 nm up to 50 μs in 200 ns bins.

single photon source, where the nth peak represents the number of coincidences between nth neighbor pulses. The peaks are separated by the period of the single photon sequence and have widths determined by the single photon shape. We calculate $g^{(2)}$ from the total number of coincidence events in each peak, $N_{\mathrm{coinc},n}$, the total number of counts in each channel, N_1 and N_2, and the number of times the sequence was repeated, N_{trig}, by

$$g^{(2)}(n) = \frac{N_{\mathrm{trig}} N_{\mathrm{coinc},n}}{N_1 N_2}, \tag{1}$$

as in Ref. [12]. N_{trig} is calculated as the total measurement time divided by the duration of a single cycle.

The data include not only correlations between single photon events but also correlations with the background noise. Therefore, we expect to measure a nonzero $g^{(2)}(0)$ depending on the signal-to-background ratio (SBR). If the signal and background are statistically independent and the intensity correlation of the background is 1, this relationship is given by

$$g^{(2)}(n) = 1 + \rho^2[g^{(2)}_{\text{signal}}(n) - 1], \quad (2)$$

where $\rho = \text{SBR}/(1 + \text{SBR})$ [22]. If a perfect single photon source is assumed [that is, $g^{(2)}_{\text{signal}}(0) = 0$], we have

$$g^{(2)}(0) = 1 - \rho^2. \quad (3)$$

The measured $g^{(2)}(n)$ for the cavity emission at 866 nm is shown in Fig. 4(a). 294 020 single photon events were detected over 180 s: an average rate of 1633 counts/s. In this time, only two coincidence events were observed at $n = 0$, giving $g^{(2)}(0) = 0.0017 \pm 0.0012$. The background count rate was measured by running the experimental sequence with no ion present in the trap. In this way, a rate of 1 counts/s was measured. Given this SBR, we expect $g^{(2)}(0) = 0.0012$; these coincidence events can therefore be fully accounted for by the background count rate.

The ion-cavity system was then connected to the QFC setup. The measured single photon rate at 1530 nm was 45.3 counts/s, with 1 325 433 total counts observed over 8.1 h. Because of background light picked up through the QFC system, the gated background count rate was 19 counts/s (again measured by running the sequence with no ion present), giving a SBR of 1.38. We observed $g^{(2)}(0) = 0.67 \pm 0.07$, as shown in Fig. 4(b), which is in agreement with the expected $g^{(2)}(0)$ value of 0.660 for this SBR. The $g^{(2)}(0)$ is significantly below the classical limit and clearly demonstrates the conversion of single photons from the ion-cavity system from 866 to 1530 nm.

To demonstrate that the nonclassical nature of the single photons is preserved even over long distances, a 10 km SMF was inserted between the QFC setup and the HBT setup. The typical attenuation through an optical fiber at 866 nm is 3 dB/km; over 10 km, this equates to a reduction in the signal by a factor of 1000. At 1530 nm, however, the attenuation is only 0.2 dB/km: a 40% reduction in the signal over the same distance. After the 10 km fiber, we observed an average rate of 21.5 counts/s. However, the background rate was also attenuated to 8.5 counts/s, resulting in an average SBR of 1.53. Using QFC, we achieve a count rate an order of magnitude greater than would be possible with the direct transmission of 866 nm. The data set shown in Fig. 4(c) includes a total of 2 081 939 counts collected over 26.9 h. From this, we extract $g^{(2)}(0) = 0.59 \pm 0.07$, in agreement with both the previous value and the calculated value of 0.634, demonstrating the preservation of sub-Poissonian statistics after transmission through the 10 km optical fiber.

Additionally, we observed the preservation of the temporal shape of the photons, an important factor in a quantum network, as efficient reabsorption requires tailored photon shapes [23]. To measure the temporal shape of the photons, we recorded their arrival time distribution at the detector with respect to the trigger signal from the pulse sequence. Histograms of these distributions for all three cases are shown in Fig. 5, which clearly demonstrates the preservation of the temporal shape for the single photons through the conversion process.

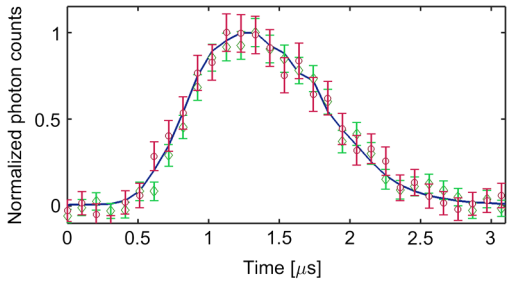

FIG. 5. The single photon shape for 866 nm, shown as a solid line, and telecom photons with and without the 10 km fiber, shown as red circles and green squares, respectively. Photon arrival times with respect to the sequence trigger are sorted into 80 ns time bins, and the resulting photon shapes are normalized to unity for comparison after subtracting the noise. The photons were collected over 1000 s for telecom and 90 s for 866 nm.

During completion of this work, we became aware of related experimental work using a trapped ion and a highly efficient polarization-independent QFC system, in which entanglement was generated between the ion and frequency converted photons [20]. While here we do not address the question of coherence of the photonic conversion, our work employs an optical cavity to allow for temporal wave packet shaping as well as converting the single photons to the more efficient telecom C band.

In this Letter, we have demonstrated the efficient frequency conversion of single photons from an ion-cavity system and the preservation of their nonclassical statistics and temporal shape through the conversion process. The agreement between the predicted and measured values for $g^{(2)}(0)$ shows that the ion-cavity system is a true single photon source, with observed coincidences being due to the background noise. Furthermore, we have shown that these features can be preserved over long distances by employing a 10 km SMF. A possible improvement to this scheme would be to produce photons of a single defined polarization by driving a Raman transition between specific Zeeman sublevels [3]. This would approximately double the efficiency of the system, as the polarization of the photons could be chosen to match the optimum polarization of the QFC system. Additionally, there is only 20% transmission through BPF2 after QFC. This could be increased to 90% using commercially available filters. With these changes, $g^{(2)}(0) < 0.5$ for up to 60 km would be expected. With a few reasonable assumptions, this value meets the requirement to establish an entanglement link between distant ions through the entanglement swapping of two telecom photons entangled with ions [24].

The techniques and results in this Letter present a wide range of opportunities. The entanglement of trapped ions

separated by 1 m has been demonstrated [27]; with QFC, this could be extended to many kilometers. Engineering the temporal shape of the photons emitted by the ion-cavity system to match those from another quantum system, and employing QFC to match the wavelengths of the systems, might provide a way to establish entanglement between disparate quantum systems. With ion-cavity systems providing superior control over the photon emission process as compared to conventional trapped ion techniques, thus making it the prime candidate for networked quantum information systems, the results presented here are a major step towards these applications.

This work was supported by CREST, JST JPMJCR1671; MEXT/JSPS KAKENHI Grants No. JP18H04291, No. JP16H02214, No. JP16H01054, No. JP15KK0164, and No. JP16K17772; and JSPS Bilateral Open Partnership Joint Research Projects. We also gratefully acknowledge support from EPSRC through the United Kingdom Quantum Technology Hub: NQIT—Networked Quantum Information Technologies EP/M013243/1 and EP/J003670/1.

[1] H.-J. Briegel, W. Dür, J. I. Cirac, and P. Zoller, Phys. Rev. Lett. **81**, 5932 (1998).
[2] M. Keller, B. Lange, K. Hayasaka, W. Lange, and H. Walther, Nature (London) **431**, 1075 (2004).
[3] H. Barros, A. Stute, T. Northup, C. Russo, P. Schmidt, and R. Blatt, New J. Phys. **11**, 103004 (2009).
[4] A. Stute, B. Casabone, P. Schindler, T. Monz, P. Schmidt, B. Brandstätter, T. Northup, and R. Blatt, Nature (London) **485**, 482 (2012).
[5] D. L. Moehring, M. J. Madsen, K. C. Younge, J. R. N. Kohn, P. Maunz, L.-M. Duan, C. Monroe, and B. B. Blinov, J. Opt. Soc. Am. B **24**, 300 (2007).
[6] N. H. Nickerson, J. F. Fitzsimons, and S. C. Benjamin, Phys. Rev. X **4**, 041041 (2014).
[7] N. Gisin and R. Thew, Nat. Photonics **1**, 165 (2007).
[8] C. Simon, Nat. Photonics **11**, 678 (2017).
[9] P. Kumar, Opt. Lett. **15**, 1476 (1990).
[10] C. Langrock, E. Diamanti, R. V. Roussev, Y. Yamamoto, M. M. Fejer, and H. Takesue, Opt. Lett. **30**, 1725 (2005).
[11] S. Tanzilli, W. Tittel, M. Halder, O. Alibart, P. Baldi, N. Gisin, and H. Zbinden, Nature (London) **437**, 116 (2005).
[12] R. Ikuta, Y. Kusaka, T. Kitano, H. Kato, T. Yamamoto, M. Koashi, and N. Imoto, Nat. Commun. **2**, 1544 (2011).
[13] R. Ikuta *et al.*, Phys. Rev. A **87**, 010301 (2013).
[14] M. T. Rakher, L. Ma, O. Slattery, X. Tang, and K. Srinivasan, Nat. Photonics **4**, 786 (2010).
[15] K. De Greve *et al.*, Nature (London) **491**, 421 (2012).
[16] A. Radnaev, Y. O. Dudin, R. Zhao, H. H. Jen, S. Jenkins, A. Kuzmich, and T. A. B. Kennedy, Nat. Phys. **6**, 894 (2010).
[17] Y. O. Dudin, A. G. Radnaev, R. Zhao, J. Z. Blumoff, T. A. B. Kennedy, and A. Kuzmich, Phys. Rev. Lett. **105**, 260502 (2010).
[18] P. Farrera, N. Maring, B. Albrecht, G. Heinze, and H. de Riedmatten, Optica **3**, 1019 (2016).
[19] R. Ikuta, T. Kobayashi, K. Matsuki, S. Miki, T. Yamashita, H. Terai, T. Yamamoto, M. Koashi, T. Mukai, and N. Imoto, Optica **3**, 1279 (2016).
[20] M. Bock, P. Eich, S. Kucera, M. Kreis, A. Lenhard, C. Becher, and J. Eschner, arXiv:1710.04866.
[21] S. Begley, M. Vogt, G. K. Gulati, H. Takahashi, and M. Keller, Phys. Rev. Lett. **116**, 223001 (2016).
[22] C. Becher, A. Kiraz, P. Michler, A. Imamoğlu, W. V. Schoenfeld, P. M. Petroff, L. Zhang, and E. Hu, Phys. Rev. B **63**, 121312 (2001).
[23] G. S. Vasilev, D. Ljunggren, and A. Kuhn, New J. Phys. **12**, 063024 (2010).
[24] See Supplemental Material at http://link.aps.org/supplemental/10.1103/PhysRevLett.120.203601, which includes Refs. [25,26], for a complete description of the model and assumptions used.
[25] R. Ikuta *et al.*, arXiv:1710.09150.
[26] Y. Tsujimoto, M. Tanaka, N. Iwasaki, R. Ikuta, S. Miki, T. Yamashita, H. Terai, T. Yamamoto, M. Koashi, and N. Imoto, Sci. Rep. **8**, 1446 (2018).
[27] D. Moehring, P. Maunz, S. Olmschenk, K. Younge, D. Matsukevich, L.-M. Duan, and C. Monroe, Nature (London) **449**, 68 (2007).